Development and Validation of a Thickened Flame Modeling Approach for Large Eddy Simulation of Premixed Combustion

Peter A. Strakey
National Energy Technology Laboratory,
US DOE,
Morgantown, WV 26507

Gilles Eggenspieler
ANSYS Inc.,
Canonsburg, PA 15317

The development of a dynamic thickened flame (TF) turbulence-chemistry interaction model is presented based on a novel approach to determine the subfilter flame wrinkling efficiency. The basic premise of the TF model is to artificially decrease the reaction rates and increase the species and thermal diffusivities by the same amount, which thickens the flame to a scale that can be resolved on the large eddy simulation (LES) grid while still recovering the laminar flame speed. The TF modeling approach adopted here uses local reaction rates and gradients of product species to thicken the flame to a scale large enough to be resolved by the LES grid. The thickening factor, which is a function of the local grid size and laminar flame thickness, is only applied in the flame region and is commonly referred to as dynamic thickening. Spatial filtering of the velocity field is used to determine the efficiency function by accounting for turbulent kinetic energy between the grid-scale and the thickened flame scale. The TF model was implemented into the commercial computational fluid dynamics code FLUENT. *Validation in the approach is conducted by comparing model results to experimental data collected in a laboratory-scale burner. The burner is based on an enclosed scaled-down version of the low swirl injector developed at Lawrence Berkeley National Laboratory. A perfectly premixed lean methane-air flame was studied, as well as the cold-flow characteristics of the combustor. Planar laser induced fluorescence of the hydroxyl molecule was collected for the combusting condition, as well as the velocity field data using particle image velocimetry. Thermal imaging of the quartz liner surface temperature was also conducted to validate the thermal wall boundary conditions applied in the LES calculations.*
[DOI: 10.1115/1.4000119]

1 Introduction

The goals of the DOE Turbines Program require the flexibility to produce clean efficient power with fuels that contain high concentrations of hydrogen. These goals include a NO_x emission target of 2 ppmv at firing temperatures that are roughly the same or higher than the current state-of-the-art gas turbine engines. The ability to design and field a fuel-flexible low emission combustor will depend largely on the understanding of fundamental combustion processes that govern such phenomenon as turbulent premixed flame propagation, flashback, and NO_x formation. It is also expected that computational fluid dynamics (CFD), including large eddy simulation (LES), will play a significant role in the development of a fuel-flexible combustor. Lean premixed combustion is a very challenging problem to model computationally. Numerous modeling approaches have been developed for premixed flames, but it is not clear that any one model is superior in predictive capabilities or that any one model is suitable across a broad range of combustion regimes, fuel types, and operating conditions.

The most common LES combustion submodels include simple extensions of Reynolds averaged Navier–Stokes (RANS) models such as the eddy-breakup model, which treats the local chemical reaction rate as the mixing rate of the finer scales of turbulence, or the progress variable model, which uses an empirical formulation of the turbulent flame speed to calculate the chemical source term.

More recent models, developed specifically for LES, include the level set, or *G*-equation approach [1], which treats the flame surface as a continuously propagating surface that is tracked by the isosurface of the scalar *G*. The *G*-equation method works well in the thin and corrugated reaction regimes but usually cannot model flames, which are discontinuous due to local quenching. The linear eddy model (LEM) [2] solves a one-dimensional mixing and diffusion problem at the subgrid level and uses finite-rate chemistry. This approach is applicable to a broader range of problems but is significantly more computationally expensive than the *G*-equation method. An even more elegant approach is the filtered density function (FDF) [3], which is a stochastic approach that uses discrete "particles" to track the mixing and diffusion of chemical species. The stochastic equations are typically solved using a Lagrangian Monte Carlo procedure resulting in a completely closed form for the reaction rates. Finite rate chemistry using simple one-step global reactions and multistep stiff reaction sets are applicable. The FDF method is applicable across a broad range of problems including nonpremixed, partially premixed, and fully premixed combustion problems. The computational demand of the three approaches described here increase significantly from the *G*-equation, to LEM, to FDF.

Another approach that has received some attention over the past decade due to its computational efficiency is the thickened flame (TF) model. The idea behind the TF modeling approach is to artificially thicken the flame-front so that it can be resolved on the

Contributed by the International Gas Turbine Institute of ASME for publication in the JOURNAL OF ENGINEERING FOR GAS TURBINES AND POWER. Manuscript received April 8, 2009; final manuscript received April 10, 2009; published online April 7, 2010. Editor: Dilip R. Ballal.

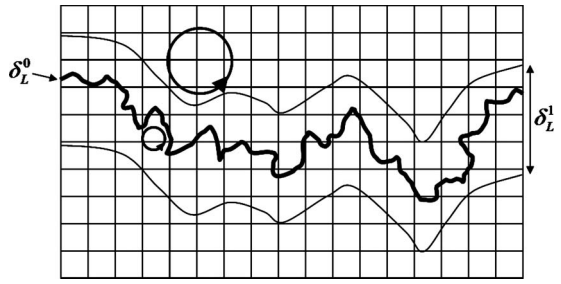

Fig. 1 Schematic of flame and turbulence scales relative to the grid scale

LES grid, while still maintaining the correct laminar flame speed and the interaction between the flame and the turbulence. The TF model was originally proposed by Butler and O'Rourke [4] who noticed (through Eq. (1)) that a premixed flame with a one-step global mechanism could be resolved on a relatively coarse grid by artificially increasing the mass thermal diffusivities, D, by some value, F, and by decreasing the reaction rate, RR, by the same amount.

$$s_L^0 \propto \sqrt{D \cdot RR}, \quad \delta_L^0 \propto \frac{D}{s_L^0} \tag{1}$$

The laminar flame speed, s_L^0, is thus maintained while the flame thickness, δ_L^0, is increased by the factor F.

In a turbulent premixed flame, the artificial thickening suppresses the interaction between the turbulence and the flame-front because only turbulent scales larger than the flame thickness can induce flame wrinkling, thereby increasing the flame surface area and turbulent flame speed. This is evident in Eq. (2) by the Damköhler number, D_a, which is a ratio between the turbulent and chemical timescales, τ_t and τ_c, based on the integral length scale, l_t, and the rms turbulent fluctuating velocity u'.

$$D_a = \frac{\tau_t}{\tau_c} = \frac{l_t s_L^0}{u' \delta_L^0} \tag{2}$$

As the flame is thickened, the Damköhler number decreases and the thickened flame does not respond to turbulent scales smaller than $\delta_L^1 = F\delta_L^0$. Figure 1 shows a typical example of the scales δ_L^0 and δ_L^1 relative to a computational grid with turbulent eddies of size Δ_x and δ_L^1. To account for the subfilter wrinkling, an efficiency function, E, is typically used to represent the flame surface area for scales smaller than the thickened flame scale, Δ_e. Following the approach of Colin et al. [5], the species and thermal molecular diffusivity are multiplied by a factor EF and the reaction rates by E/F, which maintains the thickness of the flame, regardless of the efficiency function, E.

The final form of the filtered species transport equation then becomes

$$\frac{\partial \bar{\rho} \tilde{Y}_i}{\partial t} + \frac{\partial (\bar{\rho} \tilde{Y}_i \tilde{u}_j)}{\partial x_j} = \frac{\partial}{\partial x_j}\left(\bar{\rho}\left(EFD_i + \frac{\mu_t}{\mathrm{Sc}_t} \right) \frac{\partial \tilde{Y}_i}{\partial x_j} \right) + \frac{E\tilde{\omega}_i}{F} \tag{3}$$

where ω_i is the chemical source term, Y_i is the species mass fraction, μ_t is the turbulent viscosity, and Sc_i is the species Schmidt number. In this manner, the flame-front always propagates at the speed Es_L^0 and the flame thickness remains constant at $F\delta_L^0$.

Several models for calculating E have been proposed and applied to a variety of premixed combustion problems. Collin et al. [5] derived the following expression for the efficiency function:

$$\Xi = 1 + \alpha \frac{u'_{\Delta_e}}{s_L^0} \Gamma\left(\frac{\Delta_e}{\delta_L}, \frac{u'_{\Delta_e}}{s_L^0} \right) \tag{4}$$

where

$$\alpha = \beta \frac{2\ln(2)}{3c_{ms}(\mathrm{Re}_t^{1/2} - 1)} \tag{5}$$

The model constant β is of order unity and the constant $c_{ms} = 0.28$ was derived from direct numerical simulation (DNS) data. The turbulent Reynolds number is defined as $\mathrm{Re}_t = u' l_t / \nu$. The function Γ represents the integration of the turbulent strain rate induced by the scales smaller than Δ_e and is fitted by the function

$$\Gamma\left(\frac{\Delta_e}{\delta_L}, \frac{u'_{\Delta_e}}{s_L^0} \right) = 0.75 \exp\left[-1.2 \left(\frac{u'_{\Delta_e}}{s_L^0} \right)^{-0.3} \right] \left(\frac{\Delta_e}{\delta_L} \right)^{2/3} \tag{6}$$

E is then given by

$$E = \frac{\Xi | \delta_L = \delta_L^0}{\Xi | \delta_L = \delta_L^1} \tag{7}$$

and is bounded by a minimum of 1.0 (no subfilter wrinkling) and a maximum of $F^{2/3}$. The evaluation of the velocity fluctuations at the subfilter level was proposed by Colin et al. [5] to be

$$u'_{\Delta_e} = 2\Delta_x^3 \nabla^2 (\nabla \times \vec{u}) \tag{8}$$

where the constant 2.0 is a correction factor to account for the turbulent energy found between scales Δ_x and Δ_e.

There are several difficulties in implementing the formulation of the efficiency function, as outlined by Eqs. (4)–(8) in a LES solver. First, the turbulent Reynolds number in Eq. (5) is generally not known a priori. Second, the calculation of u'_{Δ_e} requires the third derivative of the velocity field. Colin et al. [5] used a constant value of α based on an estimated Re_t for their LES simulations of a lean premixed combustor.

Durand and Polifke [6] applied the TF model to the Volvo lean premixed combustor, which is a rectangular combustor with a bluff-body flame holder. The approach they used was to thicken the flame only in the region of the flame-front using a progress variable to mark the location where thickening was applied. This is commonly referred to as dynamic thickening. They implemented the TF model in the commercial code FLUENT [7] using user-defined functions (UDFs) to calculate u'_{Δ_e} and the chemical source terms and found good agreement between the LES predictions and the experimental data for the temperature and velocity field in the combustion zone.

Other methods to estimate the subgrid flame wrinkling have also been developed and applied in LES calculations. Charlette et al. [8,9] proposed a power-law method to estimate the flame surface area based on a cutoff length scale that limits the wrinkling at the smaller scales. Fureby [10] developed a fractal method for estimating the efficiency function combined with a flamelet approach for the chemistry and applied this to the ORACLES dump combustor. More recently, De and Acharya [11] presented a comparison of the approach of Collin et al. [5] and the power law model of Charlette et al. [8] using both a dynamic and a nondynamic thickening formulation, as well as one and two-step chemistry models. Their simulations were based on the piloted premixed methane-air Bunsen burner experiments of Chen et al. [12]. Comparisons of the velocity and progress variable fields showed that in general, the dynamically thickened power-law model performed the best and that the two-step chemistry model yielded significantly better results than the one-step model.

The goal of this study is to implement the dynamically thickened flame model in the commercial code FLUENT using the efficiency function outlined by Eqs. (4)–(8) and to validate the results with experimental data collected in a laboratory-scale, swirl-stabilized, lean premixed combustor. Some unique differences in this study compared with other studies of the TF modeling approach is the use of velocity field filtering to extract the efficiency function and the use of multistep stiff chemistry. Also, the experiments for collecting validation data were conducted in such a way

as to provide well defined boundary conditions and key types of data for validating LES computations.

2 Modeling Approach

Calculation of the thickening factor, F, using a dynamic formulation requires some marker of the reaction zone so that thickening is only applied in this region as opposed to thickening the entire domain. Using one-step chemistry, Selle et al. [13] used the Arrhenius reaction rate with a reduced activation energy to thicken the reaction zone. Durand and Polifke [6] took a slightly different approach using a progress variable formulation to calculate the thickening factor. Both approaches are similar in that they broaden the reaction zone over several LES grid cells and provide ample resolution of the species and temperature fields so that gradients can be accurately calculated. The approach taken here is to use a combination of heat release rate and gradients of product species to calculate the thickening factor, F. The maximum thickening factor, $F_{\max}$, is set equal to $4\Delta_x/\delta_L^0$ and the maximum gradient of the mass fraction of the product species H_2O, $\nabla_{\max}$ is set equal to $Y_{H_2O}/(4\Delta_x)$, where Y_{H_2O} is the mass fraction of H_2O in the product gases. The two thickening factors, F_1 and F_2, are calculated by Eq. (9) and the local thickening factor, F_{loc}, is taken to be the maximum of the two.

$$F_1 = \frac{F_{\max}\nabla_{H_2O}}{\nabla_{\max}} + 1, \quad F_2 = (F_{\max} - 1)\tanh(RR/RR_{\max}) + 1$$

$$F_{loc} = \max(F_1, F_2) \tag{9}$$

In Eq. (9), RR is the local heat release rate and $RR_{\max}$ is the maximum heat release rate calculated with a one-dimensional laminar flame simulation. This formulation was found to provide good thickening in the reaction zone and ample resolution of the species and temperature gradients for both methane and hydrogen based fuels.

2.1 Efficiency Function. The initial approach for calculating u'_{Δ_e} was based on the work of Durand and Polifke [6]. A simplified version of their user-defined function was developed that was able to take advantage of the built-in macros within FLUENT for calculating gradients of the velocity field. Initial results in both reacting and nonreacting flowfields showed that u'_{Δ_e} had very large cell-to-cell variations with many cells having unphysically large values. The time-averaged values of u'_{Δ_e}(for $\Delta_e = 5\Delta_x$) were compared with U_{rms}, which is the root mean squared value of the resolved velocity field and were found to often times be significantly larger than U_{rms}. Grid resolution studies revealed that u'_{Δ_e} decreased with increasing grid resolution and that a very fine grid resolution was necessary in order to calculate u'_{Δ_e} based on Eq. (8). This is not surprising since FLUENT is a second-order accurate code and Eq. (8) requires the third derivative of the velocity field. The numerical errors associated with the calculation of Eq. (8) are very large for typical LES meshes. This issue will be illustrated later in this paper.

An alternative approach was developed based on filtering of the velocity field to extract u'_{Δ_e}. The filter adopted here is a top-hat filter built into FLUENT that involves a volume comprising the cell of interest plus the neighboring cells that share faces with the center cell. The result of applying the filter to the velocity field is the volume-weighted average velocity. For a hexahedral mesh, the ratio of the filter size to the cell size ($\tilde{\Delta}/\Delta_x$) is 1.9 ($7^{1/3}$). The size of the filter kernel can be increased by recursively filtering the velocity field n times. For the simulations conducted in this study, the flame was thickened so that the reaction zone, in a single dimension, covered approximately 5 grid cells. Recursively filtering the velocity field four times was empirically found to produce a filter kernel length of approximately $5\Delta_x$; thus the filtered velocity field represents the average over 125 (5^3) cells. The filtering process was carried out for each of the three velocity components and the filtered velocity component was subtracted from the value at the center cell and summed for the three components resulting in a velocity, u'_{Δ_e}, representative of the turbulent energy between scales Δ_x and $5\Delta_x$. As with the method proposed by Colin et al. [5] in Eq. (8), the current method using filtering also produces a dilational free form of u'_{Δ_e}.

The second and perhaps more complex part in calculating the efficiency function is the estimation of the turbulent Reynolds number in Eq. (5), $\text{Re}_t = u' l_t/\nu$. The most common approach is to assume a constant Re_t based on estimated characteristic velocity and length scales. Initial tests with this approach revealed that Re_t can have a significant effect on the solution and thus acts as a tuning parameter in which the desired solution can be obtained by adjusting Re_t. One of the goals of this study was to determine Re_t from the solution itself and remove this as a user-adjusted parameter. The determination of the local Re_t from a LES calculation in a dynamic or "on-the-fly" manner is not a trivial matter since u' and l_t are both statistically averaged quantities by definition. The approach taken here was to determine these quantities from cold-flow LES calculations. During the simulations, u'_{Δ_e} was calculated at each time step for a filter size of $5\Delta_x$ and the velocity field was monitored at several points at the dump plane of the combustor. After sufficient statistical data were collected, the average u'_{Δ_e} field was compared with the U_{rms} field and it was found that that the ratio $U_{\text{rms}}/u'_{\Delta_e}$ varied by a factor of 3–6 in the zone of the combustor where the flame was expected to exist. The local value of u' in the calculation of the local Re_t was then taken to be $4.5u'_{\Delta_e}$ during the combusting simulations. The integral length scale, l_t, was derived by fast Fourier transform (FFT) analysis of the cold-flow velocity field at the dump plane and was estimated to be ~ 6 mm. Although l_t is expected to vary across the computational domain, for the present study, l_t was assumed to be constant at 6 mm. The local value of u' as described above and the constant value of l_t were then used to calculate a local value of Re_t and α according to Eq. (5).

3 Experimental Setup

The combustor geometry studied here was a unique small-scale dump combustor using a scaled-down version of the low swirl injector (LSI) developed at Lawrence Berkely National Laboratory [14]. The design was scaled down using the recommendations of Johnson et al. [15] and was fabricated by milling a solid block of aluminum. The scaling process was conducted by using a combination of RANS and LES simulations to guide the design process. Due to the small size of the LSI and the relatively wide vane created by the milling process, the nominal 30% flow-split found in many LSI designs proved to be too large to produce the classic bowl-shaped flame. The final LSI was designed to have a nominal flow-split of 20% in order to produce a well defined flame shape.

The LSI was 15.8 mm in diameter with eight 3.2 mm wide slots at a 30 deg angle. The perforated plate was comprised of 13 holes of 1 mm diameter. The flow-split was measured by blocking off the vane side of the LSI and measuring the pressure drop across the LSI as a function of flowrate. The process was then repeated for the perforated plate side. The discharge coefficient was then determined for each side as a function of flowrate and thus the flow-split could be determined for any flowrate. The flow-split was found to be slightly dependent on overall flowrate and was 18.2% for the conditions studied here.

The injector tube had an outer diameter of 19 mm and was inserted into a machinable zirconia ceramic disk that formed the dump plane of the combustor. The zirconia had a very low thermal conductivity to provide near adiabatic conditions. The combustor wall was formed by a 46 mm internal diameter (I.D.) quartz tube,

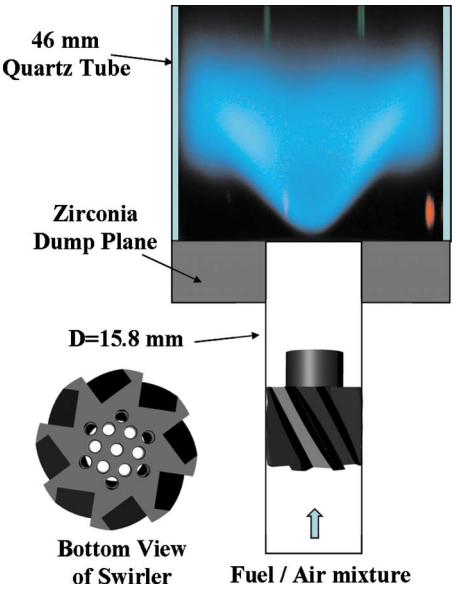

Fig. 2 Schematic of burner geometry with inset photo of flame

200 mm long with a 2 mm wall thickness. Flow conditioning upstream of the LSI was comprised of a section of 3 mm steel beads followed by a honeycomb flow straighter.

Two conditions were studied here including a cold-flow condition of 43 slpm air and hot-fire conditions of 40 slpm air and 3.0 slpm methane yielding an equivalence ratio of 0.7, which has an adiabatic flame temperature of 1840 K and a laminar flame speed of 18 cm/s based on calculations performed with the CHEMKIN laminar flame code [16] and GRI3.0 chemistry. A schematic of the burner with an inset photograph of the flame is shown in Fig. 2.

3.1 Diagnostics. Three diagnostic approaches were employed here to characterize the velocity field, flame structure, and wall temperature of the quartz tube. Velocity measurements were conducted with a commercial 2D particle image velocimetry (PIV) system from TSI Inc. (St. Paul, MN). A dual head YAG laser was used to form a laser sheet roughly 75 mm high and 0.7 mm thick passing across the centerline of the burner. Flow seeding of the air stream was accomplished using a TSI 6-jet atomizer with a slurry of yttria-stabilized zirconia particles 0.3 μm in diameter. The slurry was 30% solids by weight and was stabilized with a small amount of propylene glycol and by reducing the *p*H of the solution to 3.5. After leaving the atomizer, the slurry droplets were passed through a section of heated tubing to evaporate the water producing particulate clusters roughly 1 μm in diameter. This seeding approach was found to provide a highly controllable seeding density with excellent particle size control. The small amount of water vapor introduced into the air stream was deemed to have a negligible effect on combustion by calculating the effect on laminar flame speed and extinction strain rate.

The PIV approach consisted of using a 10 μs pulse separation time to minimize out of plane particle loss. The camera had a resolution of 2048×2048 and was fitted with a 200 mm lens located roughly 80 cm from the laser sheet to reduce perspective error caused by particles moving normal to the laser sheet due to the swirling nature of the flowfield. A Nyquist grid using a 32×32 spot size, 50% overlap, and a FFT correlating engine was used in the data reduction. With a field of view of roughly 50 mm, the corresponding spatial resolution was 0.8 mm.

The OH-planar laser induced fluorescence (PLIF) system consisted of a Quanta-Ray Pro 290 Nd:YAG laser, PDL-1 dye laser, and doubling crystal to produce ~10 ns laser pulses at 10 Hz with about 10 mJ of output per pulse at the Q1(9) line of the (1,0) band of the OH $A\ ^2\Sigma - X\ ^2\Pi$ electronic transition at 283.92 nm. This particular line was selected because it is one of the strongest transitions and has only a mild temperature dependence over the ranges of temperatures expected here. The line location was determined by scanning the dye laser through a Bunsen flame and comparing the resulting spectrum to calculations performed with the LIFBASE code [17].

The dye laser had a specified full-width half-maximum line width of 0.2 cm^{-1}, which translated to a line width of 0.3 cm^{-1} after frequency doubling.

A combination of fused silica cylindrical and spherical lenses was used to form a laser sheet approximately 75 mm high and 200 μm thick, which was directed through the center of the combustor. At the laser power density used here, the OH absorption should be well into the linear regime, far from saturation. A Princeton Instruments I-Pentamax intensified camera with a 512×512 sensor and a 45 mm *f*1.8 fused silica lens with both long-pass and band-pass filters was used to image the fluorescence signal around 310 nm while blocking most of the unwanted scattered laser light. The field of view was 50 mm^2, which yielded a resolution of 98 μm/pixel. Correction of the images due to variation in laser sheet intensity in the vertical direction was performed by imaging the laser sheet on a Uranin filter after each experiment. The fluorescence from the Uranin filter was then used to normalize the individual OH-PLIF images. A more in-depth description of the OH-PLIF setup can be found in Ref. [18].

Infrared imaging of the combustor liner was performed to collect temperature boundary conditions for use in the LES computations. An Electro-Physics IR camera with a 3–5 μm band-pass lens was used to image a 5 mm wide black strip painted axially on the outside of the quartz tube. After data were collected, the camera was calibrated with a black-body radiation source and the data were converted from pixel counts to absolute temperature.

4 Numerical Approach

The code used here is FLUENT 6.3, which is a commercial finite-volume based CFD code with a broad range of modeling capabilities. The three-dimensional computational domain encompassed the region from 2 cm upstream of the swirler to 8 cm into the combustor section and was comprised of approximately 2.9×10^6 cells, which were mostly structured hexahedral with a layer of tetrahedral cells near the walls. The grid resolution was roughly 0.1 mm in swirler region, expanding to 0.2 mm in the first 3 cm of the combustor and expanding again to 0.4 mm in the downstream area of the combustor and again to 0.8 mm near the exit of the combustor. A cross-sectional plane showing the grid cell size in millimeters is shown in Fig. 3. The leading edge of the flame was mostly located in the 0.2 mm grid resolution region.

The flow-split between the perforated plate section and swirl section was manually specified by placing a wall between the two sections and specifying the mass flowrate for each section.

The spectral synthesizer method was used to synthesize the turbulence present in the inlet stream with a turbulent kinetic energy of 5% of the mean flow and a length scale of 1 mm. The specification of the inflow turbulence parameters was found to have little effect on the solution as the swirler, which is included in the grid, generates much larger levels of turbulence. The combustor exit was modeled as a pressure outlet.

The subgrid viscosity model used here was the "localized dynamic kinetic energy model" (LDKM) [19]. The discretization scheme used for the momentum equations was a second-order accurate bounded central differencing scheme in space and a second-order backward differencing scheme was used for the temporal discretization. The bounded central differencing scheme uses pure central differencing by default but reverts to a blend of central differencing and upwinding schemes when the convection boundedness criteria are violated. All of the scalar equations were discretized using a second-order upwind scheme. The time step used was 10 μs, which corresponded to a maximum Courant–Friedrichs–Lewy (CFL) number of 1 near the inlet and about 0.2

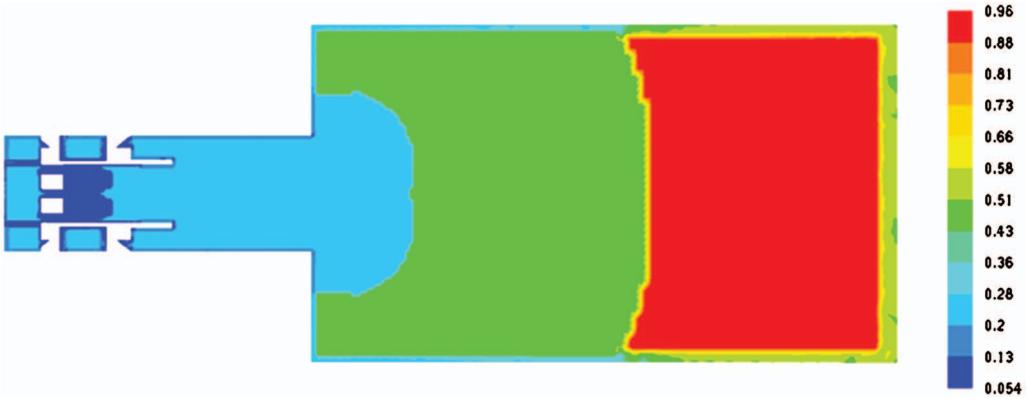

Fig. 3 Contour plot of grid cell size (mm). Cutting plane through center of combustor.

in the combustor. The simulations were run for about 50 ms, which corresponded to about 25 flow-through times of the nozzle section. This was found to be more than adequate to obtain good statistical quantities.

4.1 Chemistry. Simulations were performed with a global methane-air one-step reaction, $CH_4+2O_2 \rightarrow CO_2+2H_2O$, where the reaction rate is given by $RR=A[CH_4]^{0.2}[O_2]^{1.3}\exp(E_a/RT)$, with $A=1.74\times10^{13}$ and $E_a=2.027\times10^5$ J/mole. This is the default methane-air mechanism built into FLUENT with the pre-exponential factor adjusted to reproduce the estimated flame speed of 18 cm/s. A second chemistry mechanism, based on the four-step methane-air augmented reduced mechanism of Seshadri and Peters [20], was also used.

$$CH_4 + 2H + H_2O \rightarrow CO + 4H_2$$

$$CO + H_2O = CO_2 + H_2$$

$$2H + M \rightarrow H_2 + M$$

$$O_2 + 3H_2 = 2H + 2H_2O \tag{10}$$

This mechanism was reduced from a 25-step mechanism using asymptotic analysis and assuming quasi-steady-state behavior for several of the intermediate species involved in fast shuffle reactions. The concentration of OH is calculated from the partial-equilibrium assumption $[OH]=[H][H_2O]/([H_2]K_3)$ [21].

In is important to note that this mechanism is computationally stiff and involves two reversible reactions. Since prior work using the TF model has been limited to one- and two-step simple reaction mechanisms, it was important to validate the effect of thickening on the stiff chemistry set used here. One-dimensional laminar flame calculations were performed using the reaction set given by Eq. (10). A constant thickening factor of 10 was first used, which yielded very good agreement for laminar flame speed compared with the nonthickened calculations performed on a grid with a resolution a factor of 10 smaller. Next, the dynamic thickening approach described above using gradients of H_2O was applied to the one-dimensional problem and the calculated laminar flame speed was within 5% of the nonthickened flame. The calculations validated the ability of the TF model to capture flame speed with a stiff chemistry set involving intermediate and radical species.

Combusting LES calculations were also performed with the eddy-breakup (EBU) and laminar modeling approaches, which are two of the built-in combustion models in FLUENT. The EBU model is a widely utilized approach in RANS simulations and is implemented in FLUENT by replacing the turbulent time and length scales with their corresponding subgrid values for application to LES. The EBU model assumes that the reaction rate is the lesser of the chemical kinetic and subgrid turbulent mixing rates. The laminar approach assumes infinitely fast subgrid mixing where the reaction rate is simply the chemical kinetic rate. This approach is akin to having no subgrid turbulence-chemistry interaction model.

5 Results and Discussion

5.1 Cold-Flow Simulations. In order to assess the adequacy of the grid and flow solver to predict the velocity field, cold-flow simulations were first performed for an air flowrate of 43 slpm, which corresponds to a bulk flow velocity of 3.8 m/s in the injector tube. The simulation was run for 40,000 time steps or 0.4 s of physical time to obtain good mean and rms velocity statistics for comparison with the experiments. Comparison of radial profiles of mean axial velocity and rms axial velocity is presented in Fig. 4 at four different axial locations, Z, from the dump plane. As can be seen in the figure, the comparison between experiment and simulation is very good. This was somewhat expected since the computational domain encompasses the swirler and is thus insensitive to the inlet boundary conditions other than the flow-split, which was experimentally determined and used as input for the simulation. Also, the grid resolution is very good for the relatively low turbulent Reynolds number studied here with better than 90% of the total turbulent energy being explicitly resolved.

To illustrate the effect of approach for calculating the subfilter fluctuating velocity, u'_{Δ_e} was calculated using both the approach of Colin et al. [5] (Eq. (8)) and the filtering approach developed here. Figure 5 shows radial plots of $U_{\rm rms}$, u'_{Δ_e} calculated according to Eq. (8) and u'_{Δ_e} calculated using the filtering technique developed in this study at an axial location of 1.5 mm from the dump plane. The three turbulent fluctuating velocities were averaged in time and also averaged circumferentially to further smooth the values. As can be seen in the figure, Eq. (8) produces u'_{Δ_e} values that are in some locations significantly larger than $U_{\rm rms}$, which is unphysical since $U_{\rm rms}$ accounts for all of the resolved turbulent energy at all scales. The u'_{Δ_e} calculated using the filtering technique produces values that are always less than $U_{\rm rms}$ and thus physically bounded to realistic values.

5.2 Experimental Combusting Results. For the case studied here (40 slpm air, 3 slpm CH_4, $\phi=0.7$) 100 OH-PLIF images and 150 PIV image pairs were collected through the centerline of the combustor. Figure 6 shows six individual snapshots of OH-PLIF intensity corrected for laser sheet intensity distribution. The dump plane with the injector opening is annotated on the bottom of the figures. The leading edge of the flame-front can clearly be seen by the steep gradient in fluorescence intensity. The snapshots give a good idea of the degree of wrinkling in this flame and the overall shape of the flame.

Figure 7 shows the averaged velocity vectors colored by the mean axial velocity overlaid with contours of mean OH signal

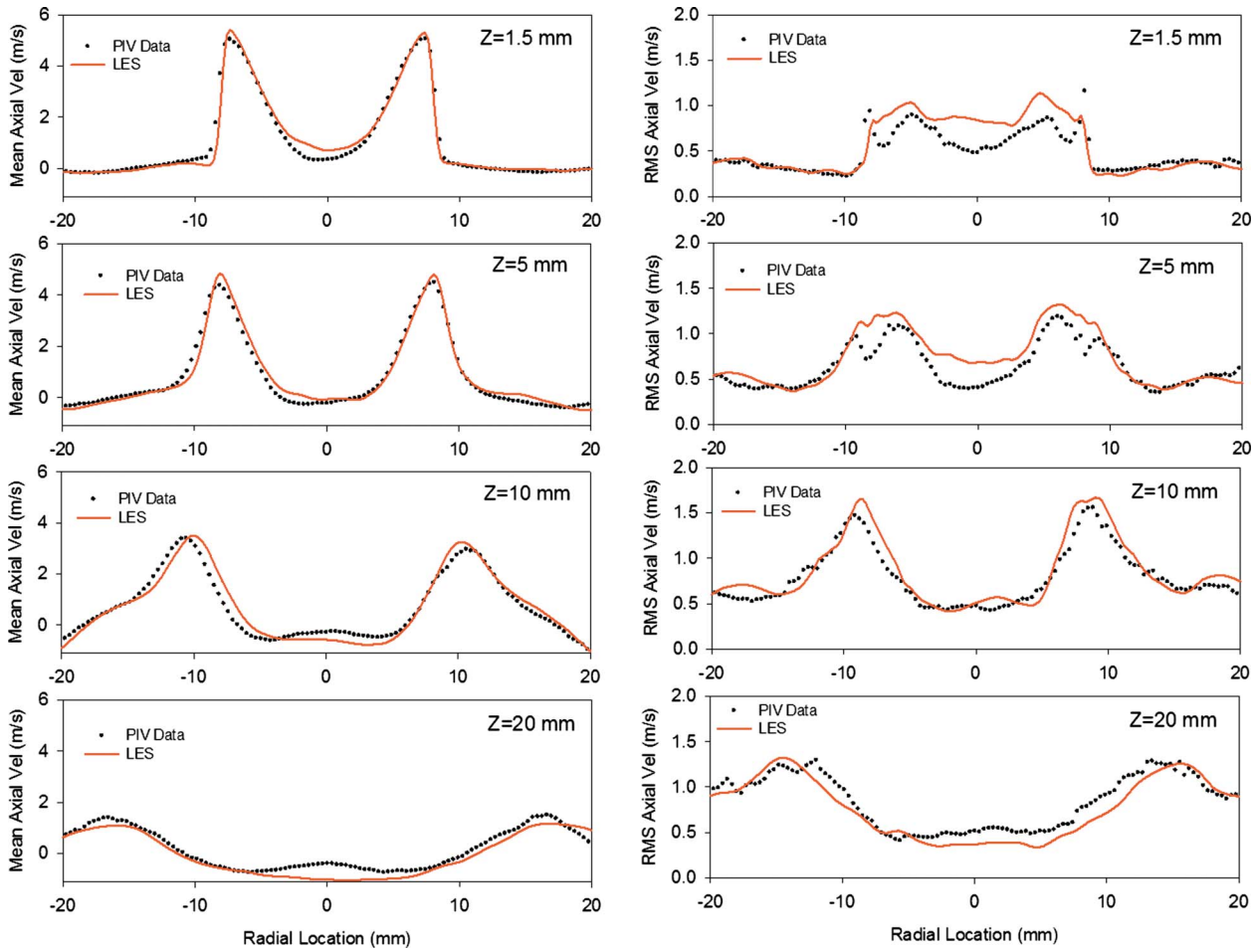

Fig. 4 Radial profiles of mean axial velocity (left) and rms axial velocity (right) at axial locations of 1.5 mm, 5 mm, 10 mm, and 20 mm for the LES calculation and PIV data

intensity and can be compared with the time-averaged chemiluminescence flame picture in Fig. 2. For purposes of clarity, only every fourth vector is shown. The OH contours are a maximum for the central contour and decrease by a factor of 2 for each expanding contour. The flame exhibits the classic features of any LSI generated methane flame with an aerodynamically stabilized bowl-shaped leading edge flame and a weak central recirculation zone. A corner recirculation zone can also be seen, which is due to the combination of the sudden expansion and the enclosed nature of the combustor.

To gain a better understanding of what regime of combustion is occurring in the present experiment, several key parameters were estimated. The Zeldovich laminar flame thickness $\delta_L = \nu / s_L$, with $s_L = 18$ cm/s is estimated to be 87 μm. The Kolmogorov length scale, $\eta_0 = l\ \mathrm{Re}_l^{-0.75}$ was estimated using a value of $u' = 1.0$ m/s, which was derived from the PIV data and the integral length scale of 6 mm as discussed above. Re_t was estimated to be $\mathrm{Re}_t = 375$ and η_0 was estimated to be 70 μm. The Karlovitz number δ_L / η_0 was estimated to be Ka = 1.25. According to the Borghi turbulent pre-

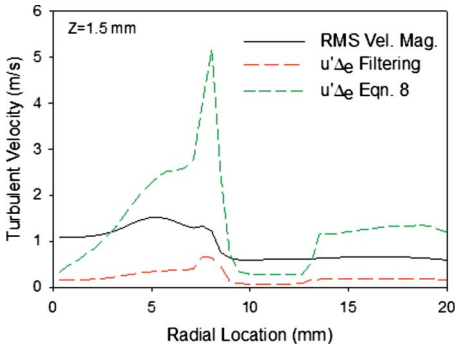

Fig. 5 Radial profiles of rms fluctuating velocity and fluctuating velocity at the filter scale using Eq. (8) and the current filtering method from a cold-flow LES calculation

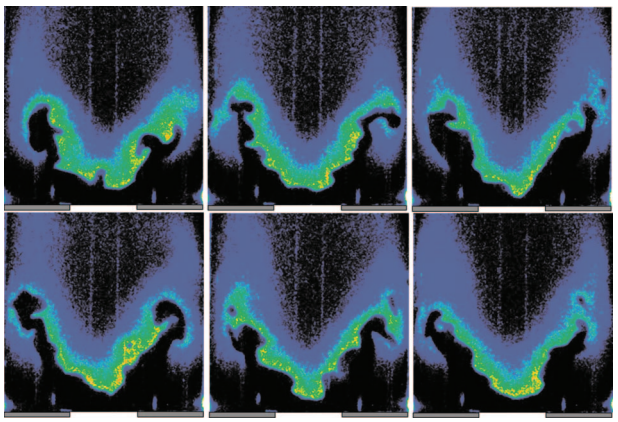

Fig. 6 Six snapshots of instantaneous OH fluorescence intensity, $\phi = 0.7$

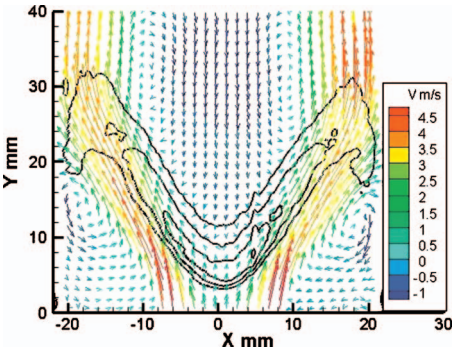

Fig. 7 Measured velocity vectors colored by mean axial velocity overlaid with measured OH fluorescence intensity contours. Central contour at maximum OH intensity.

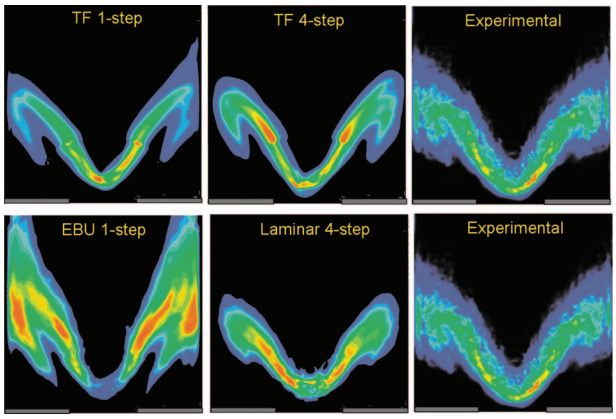

Fig. 8 Mean heat release from TF one-step, TF four-step, EBU one-step, laminar four-step simulations and experimentally derived average heat release

mixed combustion diagram, the current experiments would reside on the border between the flamelet regime and the thickened flame regime.

Although the conditions studied here are somewhat lower in turbulent Reynolds number than previous studies validating the TF modeling approach, the current experimental configuration provides an attractive geometry to validate the modeling approach due the relatively small physical size of the combustor, allowing for small grid cell sizes and modestly low levels of thickening and subfilter wrinkling. Also, the current LSI combustor lends itself well to the collection of detailed laser diagnostic data and boundary condition information.

5.3 Modeling Results. As was mentioned earlier, thermal imaging of the outside of the quartz combustor was performed to supply thermal boundary conditions for the LES computations. Since the inside wall temperature is the necessary boundary condition, a steady-state RANS simulation was performed to determine the inside wall temperature. The RANS simulation was conducted with a well resolved wall boundary layer, a finite thickness combustor wall, and a three-band radiation model to accurately predict the inner-wall temperature. The absorption coefficient of the quartz, along with the convection coefficient on the outside of the combustor wall, was adjusted until good agreement between the RANS prediction and the measured outside wall temperature was reached. The RANS prediction of the inside wall temperature as a function of axial location was then used for the LES calculations. The RANS simulation was also used as the starting point for the LES runs.

Typically, 10,000 time steps were required to flush-out the RANS solution and reach a statistically steady-state solution as monitored by the flame leading edge location and mean species concentrations. Thickening factors were typically in the range of 4–10, while the efficiency factors were in the range of 1–2. The value of α (Eq. (5)) was found to vary from 0.03 to 2.0 in the flame zone.

Since the one-step chemistry model does not provide information on OH concentration, which could be directly compared with the experimental data, an approach using the gradients of the experimentally measured OH intensity was used to develop a map of the flame-front location from each OH-PLIF image [18]. The flame-front maps were then averaged to yield a probability density function of the flame-front location, which could then be compared with the time-averaged heat release field computed from the LES computations. Figure 8 presents a comparison of the experimentally measured flame-front probability to the time-averaged heat release from the EBU one-step model, the laminar four-step approach along with the one-step and one-step TF model simulations. No scale is provided as the images are normalized by the maximum value for each image. The poor prediction of the EBU one-step model is due to the inability of this model to predict the propagation of a laminar or even low turbulence intensity premixed flame. As the subgrid turbulence approaches zero, the EBU model predicts zero reaction rate as the reaction is limited by the lesser of the kinetic rate and the subgrid turbulent mixing rate. As the subgrid turbulence increases downstream of the leading edge of the flame, the reaction rate increases resulting in a much longer flame brush. The laminar four-step model did a fairly good job of predicting heat release but did show a slightly larger standoff distance from the dump plane to the leading edge of the flame brush. Since the laminar model assumes infinitely fast subgrid mixing, one would expect the model to overpredict the reaction rates. The good agreement observed here is likely due to the relatively fine grid (0.2 mm in the flame zone) combined with inherent numerical diffusion allowing the reaction zone and scalar gradients to be partially resolved. This approach would not likely work as well on a coarser "engineering" grid where the cell size is typically an order of magnitude larger than the flame thickness. Both the one-step and four-step TF models did a good job of predicting the mean location of the flame-front compared with the experimental data. The fact that the one-step model performed equally, as well as the four-step model, is not surprising since the pre-exponential factor was tuned to reproduce the correct flame speed of 18 cm/s, which was inherently predicted by the four-step mechanism. Also, the relatively low levels of $u'/S_L \sim 5$ are indicative of the linear relation between turbulent fluctuating velocity and flame surface area where local flame quenching is not likely to be an issue.

Since the four-step mechanism does provide an algebraic expression for OH concentration through the partial-equilibrium assumption discussed earlier, a more direct comparison can be made to the experimental data. Figure 9 compares the time-averaged OH fluorescence field, normalized to a maximum of 1, to the time-averaged OH mole fraction from the TF and laminar model computations. The comparison between experiment and models is very good near the leading edge of the flame with the laminar approach showing a slightly larger standoff distance as mentioned previously. The computations do, however, overpredict the OH concentration in the postflame zone and near the walls of the combustor. This is likely due to the inability of the partial-equilibrium assumption of the four-step chemistry model to accurately predict OH concentration in these regions. One dimensional laminar flame calculations did, in fact, show the four-step model to predict a slower rate of OH consumption in the postflame zone compared with GRI3.0 and the four-step mechanism predicted an equilibrium concentration two to three times higher than GRI 3.0 depending on temperature.

The velocity field is another means of validating the modeling approach that incorporates the effects of mean flow, turbulence, and heat release together. Figure 10 contains radial plots of mean

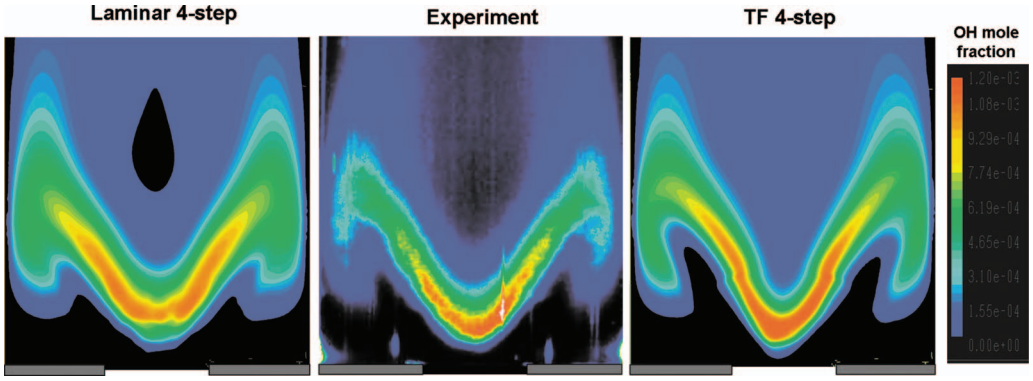

Fig. 9 Mean OH fluorescence (center) and mean OH concentration from laminar four-step (left) and TF four-step (right) LESs

axial velocity through the centerline of the combustor for all four of the LES calculations and the experimental data at four axial locations. The coordinate, Z, is the distance downstream from the dump plane. Both the one-step and four-step chemistry models incorporated into the TF model do an excellent job of predicting mean axial velocity at all four axial locations shown in the figure. The EBU one-step simulation did not show such good agreement due to the poor heat release prediction as discussed earlier. The laminar four-step simulation performed equally, as well as the TF model simulations, in predicting mean axial velocity.

The TF and laminar model simulations tend to predict a slightly lower degree of radial divergence of the flame as evidenced by the peaks in the axial velocity profiles occurring at slightly inward radial locations for the axial locations of 10 mm and 20 mm. It is not clear why this is since the agreement between the TF simulations and the PIV data is very good at axial locations of 1.5 mm and 5 mm. One possibility is that the tangential velocities, which were not measured here, are not in such good agreement.

Figure 11 contains radial plots of rms fluctuating axial velocity through the centerline of the combustor for all four of the LES calculations and the experimental data at four axial locations. Note that for the LES calculations, only the resolved portion of the fluctuating velocity is reported here. This is justified as the cold-flow simulations showed that better than 90% of the turbulent kinetic energy was being resolved by the grid. As with the mean velocity plots shown in Fig. 10, the agreement between the TF model simulations and the experimental data is quite good, while the EBU one-step simulation was somewhat less in agreement. The laminar four-step model also did a reasonably good job in predicting the rms axial velocity except for the axial location of 10 mm, where the rms velocity is overpredicted at the centerline. This is a result of large temporal fluctuations in the flame standoff distance, which was very close to 10 mm from the dump plane.

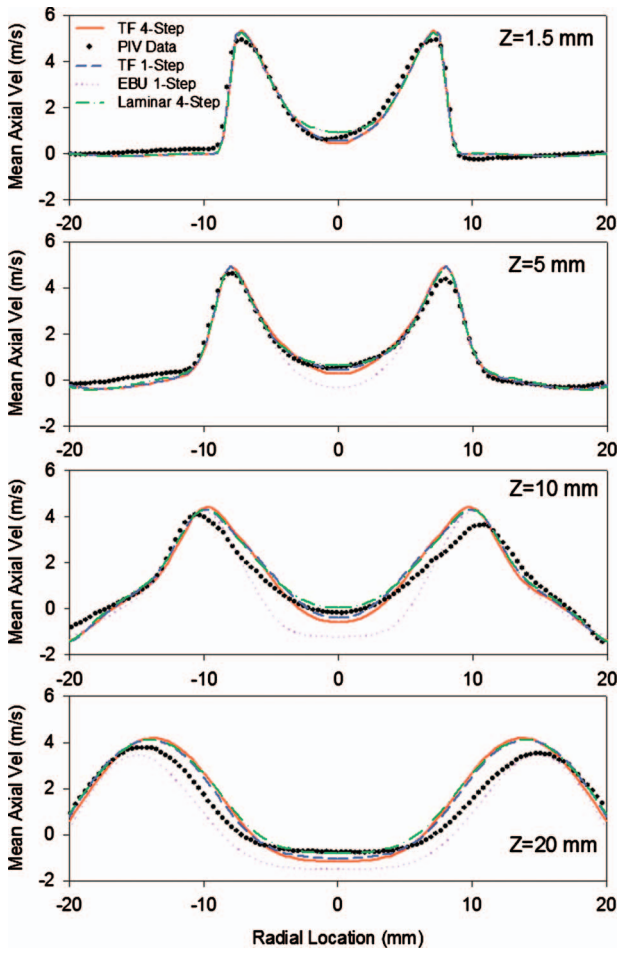

Fig. 10 Radial plots of mean axial velocity for the four LES calculations along with the PIV data at axial locations of 1.5 mm, 5 mm, 10 mm, and 20 mm (top to bottom)

6 Conclusions

The implementation of the TF model studied here using a velocity filtering technique has proven to be quite good in terms of validation with the experimental data for the conditions studied here. The velocity field was well predicted for both the cold-flow and combusting cases, while the combustion characteristics quantified by heat release and OH concentration were in good agreement with the experimental data. Both the one-step and four-step chemistry models did an excellent job of representing the chemical kinetics, which was somewhat expected since the one-step model was tuned to produce the correct laminar flame speed and the relatively low levels of u'/S_L ensure that local flame quenching is not a major feature of the combustion process. The velocity filtering technique developed here produced much more realistic values of u'_{Δ_e} compared with the formulation of $u'_{\Delta_e} = 2\Delta_x^3 \nabla^2(\nabla \times \bar{u})$. Simulations using a one-step EBU model were clearly inferior, while the four-step laminar chemistry approach, where subgrid turbulence-chemistry interactions are neglected, performed reasonably well with the small cell size (relative to the flame thickness) used in the current study.

Current efforts include the application of the TF model to large-scale combustors with much larger turbulent Reynolds number.

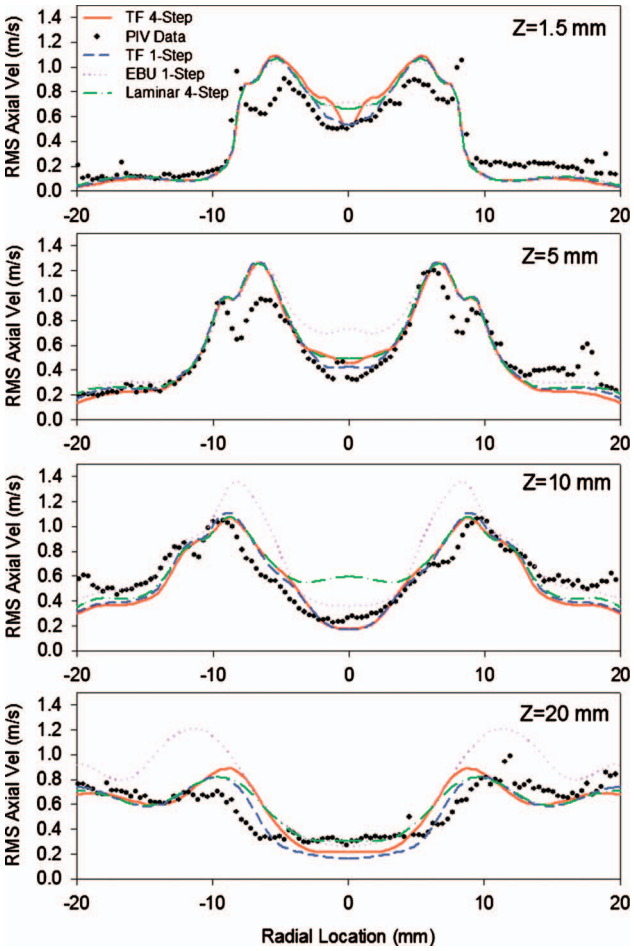

Fig. 11 Radial plots of rms axial velocity for the four LES calculations along with the PIV data at axial locations of 1.5 mm, 5 mm, 10 mm, and 20 mm (top to bottom)

Also, the TF model is currently being tested with a wide range of fuel blends including hydrogen, which is of particular interest for syngas combustion.

Acknowledgment

The authors would like to acknowledge the DoE Advanced Research Program for financial support of this work. The authors would also like to thank Ludovic Durand and Wolfgang Polifke (TU Munich) for sharing their TF model UDF. Also, the help of Dr. Graham Goldin (ANSYS Inc.) is also greatly appreciated in constructing the UDFs used to implement the TF model.

References

[1] Pitsch, H., and DuChamp De Lageneste, L., 2002, "Large-Eddy Simulation of Premixed Turbulent Combustion Using a Level-Set Approach," Proc. Combust. Inst., **29**, pp. 2001–2008.
[2] Chakravarthy, V. K., and Menon, S., 2001, "Linear Eddy Simulations of Reynolds Number and Schmidt Number Effects on Turbulent Mixing," Phys. Fluids, **13**(2), pp. 488–499.
[3] Drozda, T. G., Sheikhi, M. R. H., Madnia, C. K., and Givi, P., 2007, "Developments in Formulations and Application of the Filtered Density Function," Flow, Turbul. Combust., **78**, pp. 35–67.
[4] Butler, T. D., and O'Rourke, P. J., 1977, "A Numerical Method for Two Dimensional Unsteady Reacting Flows," Proc. Combust. Inst., **16**, pp. 1503–1515.
[5] Colin, O., Ducros, F., Veynante, D., and Poinsot, T., 2000, "A Thickened Flame Model for Large Eddy Simulations of Turbulent Premixed Combustion," Phys. Fluids, **12**(7), pp. 1843–1863.
[6] Durand, L., and Polifke, W., 2007, "Implementation of the Thickened Flame Model for Large Eddy Simulation of Turbulent Premixed Combustion in a Commercial Solver," ASME Paper No. GT2007-28188.
[7] FLUENT, ANSYS Inc.
[8] Charlette, F., Meneveau, C., and Veynante, D., 2002, "A Power-Law Flame Wrinkling Model for LES of Premixed Turbulent Combustion, Part 1: Non-Dynamic Formulation and Initial Tests," Combust. Flame, **131**, pp. 159–180.
[9] Charlette, F., Meneveau, C., and Veynante, D., 2002, "A Power-Law Flame Wrinkling Model for LES of Premixed Turbulent Combustion, Part 2: Dynamic Formulation," Combust. Flame, **131**, pp. 181–197.
[10] Fureby, C., 2005, "A Fractal Flame-Wrinkling Large Eddy Simulation Model for Predicting Premixed Turbulent Combustion," Proc. Combust. Inst., **30**, pp. 593–601.
[11] De, A., and Acharya, S., 2008, "Large Eddy Simulation of Premixed Combustion With a Thickened-Flame Approach," ASME Paper No. GT2008-51320.
[12] Chen, Y. C., Peters, N., Schneemann, G. A., Wruck, N., Renz, U., and Mansour, M. S., 1996, "The Detailed Flame Structure of Highly Stretched Turbulent Premixed Methane-Air Flames," Combust. Flame, **107**, pp. 233–244.
[13] Selle, L., Lartigue, G., Poinsot, T., Koch, R., Schildmacher, K.-U., Krebs, W., Prade, B., Kaufmann, P., and Veynante, D., 2004, "Compressible Large Eddy Simulation of Turbulent Combustion in Complex Geometry on Unstructured Meshes," Combust. Flame, **137**, pp. 489–505.
[14] Yegian, D. T., and Cheng, R. K., 1998, "Development of a Lean Premixed Low-Swirl Burner for Low NOx Practical Applications," Combust. Sci. Technol., **139**, pp. 207–227.
[15] Johnson, M. R., Littlejohn, D., Nazeer, W. A., Smith, K. O., and Cheng, R. K., 2005, "A Comparison of the Flowfields and Emissions of High-Swirl Injectors and Low-Swirl Injectors for Lean Premixed Gas Turbines," Proc. Combust. Inst., **30**, pp. 2867–2874.
[16] Lutz, A., Kee, R., Miller, J., Dwyer, H., and Oppenheim, A., 1988, 22nd Symposium (International) on Combustion, pp. 1683–1693.
[17] Luque J., and Crosley, D. R., 1999, "LIFBASE: Database and Spectral Simulation (Version 1.5)," SRI International Report No. MP 99-009.
[18] Strakey, P. A., Woodruff, S. D., Williams, T. C., and Schefer, R. W., 2008, "OH-Planar Fluorescence Measurements of Pressurized, Hydrogen Premixed Flames in the SimVal Combustor," AIAA J., **46**(7), pp. 1604–1613.
[19] Kim, W., and Menon, S., 1999, "An Unsteady Incompressible Navier-Stokes Solver for Large Eddy Simulation of Turbulent Flows," Int. J. Numer. Methods Fluids, **31**, pp. 983–1017.
[20] Seshadri, K., and Peters, N., 1988, "Asymptotic Structure and Extinction of Methane-Air Diffusion Flames," Combust. Flame, **73**, pp. 23–44.
[21] Peters, N., and Williams, F. A., 1987, "The Asymptotic Structure of Stoichiometric Methane-Air Flames," Combust. Flame, **68**, pp. 185–207.